Vibrational Spectrum of the J-625 Intermediate in the Room Temperature Bacteriorhodopsin Photocycle

G. H. Atkinson,* L. Ujj, and Yidong Zhou

Department of Chemistry and Optical Science Center, University of Arizona, Tucson, Arizona 85721

Received: June 4, 1999; In Final Form: August 27, 1999

The vibrational spectrum (800−1700 cm^{-1} region) of the J-625 intermediate, formed within 200−500 fs (3.5 ps decay time to K-590) in the room-temperature bacteriorhodopsin (BR) photocycle, is measured via picosecond time-resolved coherent anti-Stokes Raman spectroscopy (PTR/CARS). An examination of the excitation conditions and BR photocycle kinetics, as well as the vibrational CARS data, convincingly demonstrates that these PTR/CARS spectra can be quantitatively analyzed in terms of primarily BR-570 and J-625 by using third-order nonlinear susceptibility ($\chi^{(3)}$) relationships. The resultant background-free (Lorentzian line shapes) CARS spectrum contains 24 distinct vibrational features which provide the most complete structural characterization of J-625 yet reported. Comparisons of the J-625 vibrational spectrum with those of ground-state BR-570 and the K-590 intermediate show that J-625 maintains some structural similarities with BR-570 while it has a significantly different structure than that of K-590. Specifically, J-625 has (i) an all-*trans* retinal configuration, (ii) increased electron density in the C═C stretching modes as manifested by increased C═C stretching frequencies relative to those in both BR-570 and K-590, (iii) significant delocalized hydrogen out-of-plane motion not observed in any other BR species, (iv) decreased $C-CH_3$ in-plane wagging motion, and (v) a Schiff-base bonding environment similar to that of BR-570 and distinctively different from that in K-590. Comparisons between the PTR/CARS spectra of J-625 and T5.12, an intermediate found in the photoreaction of the artificial BR pigment, BR5.12, containing a five-membered ring spanning the $C_{12}-C_{13}═C_{14}$ bonds (thereby blocking $C_{13}═C_{14}$ isomerization), support the conclusion that the J-625 structure reflects the reaction coordinates in the BR photocycle that precede $C_{13}═C_{14}$ isomerization. Since these PTR/CARS data show J-625 to have an all-*trans* retinal, $C_{13}═C_{14}$ isomerization cannot be the primary reaction coordinate described in numerous models for the BR photocycle. The all-*trans* to 13-*cis* isomerization must occur as J-625 transforms into K-590, and other changes in the retinal structural and/or retinal−protein interactions must comprise the primary reaction coordinates that precede $C_{13}═C_{14}$ isomerization. These results require that significant changes in the mechanistic model describing the room-temperature BR photocycle be considered.

Introduction

The exceptionally high efficiency with which the room-temperature bacteriorhodopsin (BR) photocycle stores absorbed light energy has motivated numerous studies of its underlying molecular mechanism.[1,2] Of special importance has been an elucidation of the time-dependent changes in the retinal chromophoric structure and the corresponding interactions of the retinal with the protein environment. Independently, the BR photocycle has long been considered as a useful model for the irreversible rhodopsin (Rh) photoreaction which sustains visual processes in vertebrates and many invertebrates.[2] Mechanistic information derived from the BR photocycle has often been transferred by analogy to an understanding of the Rh photoreaction.

A significant amount of spectroscopic and kinetic data describing the BR photocycle has been reported from transient absorption measurements.[2−10] Vibrational spectra, measured at either room or low (i.e., frozen samples) temperatures, from intermediates comprising the latter part of the BR photocycle beginning with K-590 have also been reported.[11,12] The molecular processes comprising the initial stages of the BR photocycle preceding the formation of K-590, however, have not been fully characterized, especially with respect to structural changes in either the retinal chromophore or the protein binding pocket surrounding the retinal. These initial stages have been identified and kinetically characterized largely by femto/picosecond transient absorption (FTA/PTA) spectroscopy,[4−9] data which provide little, if any, direct structural information.

In the widely accepted molecular mechanism describing the early femto/picosecond events, the I-460 intermediate is thought to represent an excited electronic state while the electronic state properties (excited or ground) of J-625 remain unclear. The transient absorption data[1,2,13] used to establish the presence and kinetic properties of both I-460 and J-625 show that I-460 precedes J-625 which subsequently decays to K-590 (Figure 1). The absorption spectrum of I-460 is exceptionally broad with signals appearing from 460 to 860 nm, while absorption spectrum of J-625 appears between 600 and 800 nm.[2,8,14]

The central mechanistic roles proposed for both I-460 and J-625 in the BR photocycle require detailed characterizations of the retinal structures and the retinal−protein interactions in each species. While the kinetic properties identifying I-460 and J-625 are derived from FTA/PTA studies, the vibrational data needed to determine structures are not generally available and, indeed, are exceptionally difficult to obtain experimentally. Time-resolved infrared absorption data have been reported for a few selected bands,[15] but vibrational spectra in which normal modes can be identified are not available. For example, to measure vibrational Raman scattering during the short lifetimes of I-460 (200−500 fs) and J-625 (3.5 ps) requires correspond-

* To whom correspondence should be addressed.

10.1021/jp9918306 CCC: $19.00
Published on Web 10/23/1999

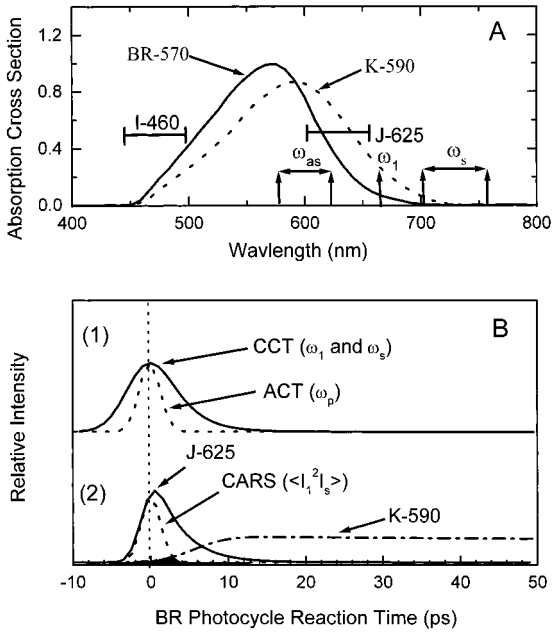

Figure 1. (A) Absorption cross-section of native BR-570 (solid line) and its intermediate K-590 (dashed line). The general spectral region in which the absorption maxima of the intermediates I-460 and J-625 are shown as "|—|". The CARS experimental wavelengths of ω_1 and ω_s, together with the respective CARS signal, ω_{as}, also are shown. (B) (1) Schematic representatives of the cross-correlation time (CCT, ~8 ps fwhm), defined by the probe laser pulses ω_1 and ω_s, and the autocorrelation time (ACT, ~3 ps fwhm) of the pump laser pulse, ω_p. (2) Schematic representatives of the transient populations for J-625 (solid line) and K-590 (dashed−dot line) are shown. The dotted line represents the third-order cross-correlation function ($\langle I_1^2 I_s \rangle$) while the shaded area shows the overlap of the K-590 population present during the time interval defined by $\langle I_1^2 I_s \rangle$.

ingly short laser pulses which generate vibrational features with exceptionally broad spectral bandwidths containing relatively little vibrational mode information. While subpicosecond laser pulses are extremely useful for transient absorption spectroscopy, laser pulses <2 ps are not particularly useful for direct measurements of vibrational (including CARS) spectra since the corresponding vibrational bandwidths (~7 cm^{-1}) are large enough to obscure much of the information provided by the vibrational degrees of freedom. For example, a recent resonance Raman study using 1 ps pulsed excitation has reported specific vibrational modes assignable to I-460, but with bandwidths of ~60 cm^{-1}.[16]

Even in the absence of vibrational data, there has been extensive discussion of the roles of I-460 and J-625 in the structural transformations (retinal and chromophore) that comprise the early stages of the BR photocycle.[4,8,17] Of particular interest has been whether C_{13}═C_{14} isomerization, or some related twisting/distortion of the C_{13}═C_{14} bond, is present in J-625 or only when K-590 appears (vibrational spectra show that K-590 contains a 13-*cis* retinal[12]). The structural characterization of J-625 directly from its vibrational spectroscopy is the focus of the work described in this paper. Special attention is given to determining the retinal configuration found in J-625 in order to establish when C_{13}═C_{14} isomerization occurs.

Essentially all current mechanistic models describing the BR photocycle at room temperature include isomerization around the C_{13}═C_{14} bond (all-*trans* to 13-*cis*) as the primary reaction coordinate.[2,18,19] Early models suggested that C_{13}═C_{14} bond isomerization (forming a 90°, twisted retinal) occurs within the excited electronic state of BR-570 upon the 200 fs decay of the Franck−Condon states populated by absorption.[4,8] The absence of emission during the initial 500 fs of the BR photocycle, however, does not support this conclusion.[17,20] Independently, calculations involving the mixing of the lowest energy ^1B_u and ^1A_g states suggest that C_{13}═C_{14} bond isomerization occurs in BR only when these two electronic states mix strongly via the torsional motion of the C_{13}═C_{14} bond.[21]

The proposal that the primary reaction coordinate involves C_{13}═C_{14} bond isomerization also has been examined in artificial BR pigments containing a structurally modified retinal designed to selectively restrict C−C═C bond motion.[22,23] Femtosecond absorption spectroscopy from such an artificial BR pigment in which C_{13}═C_{14} bond isomerization cannot occur (BR5.12) demonstrates that an intermediate (T5.12) analogous to J-625 in the native BR photocycle appears, thereby suggesting that the primary reaction coordinate(s) is not C_{13}═C_{14} bond isomerization.[22] This conclusion is supported by atomic force measurements of structural changes in the BR photocycle.[23]

Recent *ab initio* calculations[24] for a protonated Schiff base with three C═C bonds emphasize the importance of C−C/C═C bond stretching and twisting as preliminary motion prior to C═C isomerization.[24] These calculated results are consistent in the important contributions of the charge environment near the retinal as controlled by the adjacent amino acids.[25] Thus, although it is clear that C_{13}═C_{14} bond isomerization is a critical part of the overall BR photocycle, it is evident that the primary molecular events remain to be determined.

The PTR/CARS methods used here represent a compromise between the laser pulse resolution needed to separately monitor I-460, J-625, and K-590 in time, the resonance enhancements required to generate high S/N vibrational data, and the spectral resolution (bandwidth) which preserves useful vibrational mode information. The PTR/CARS measurements are made within the cross-correlation time (CCT) of 6.5 ps during which period the transient population could contain contributions from the intermediates I-460, J-625, and K-590 in addition to that from ground-state BR-570. A quantitative analysis of the kinetic, absorption, and vibrational data, however, shows that both the I-460 and K-590 contributions to the PTR/CARS spectrum at CCT are minimal, thereby making it feasible to analyze the PTR/CARS data in terms of J-625 and BR-570 in order to derive the CARS spectrum of J-625 alone.

Experimental Section

A. Materials. The BR samples, obtained from a cell line of *Halobacterium salinarium* and purified according to established procedures,[26] are buffered at pH = 7 in a water solution (17 °C) and have an optical density adjusted to 2. PTR/CARS data are recorded from a flowing BR sample created in a nozzle.

B. Instrumentation. The instrumentation and experimental procedures used to record PTR/CARS spectra are discussed in detail elsewhere[12,27] and therefore only a brief description is presented here. The 1053-nm output (30-ps pulse at 76-MHz repetition rates) of a cw, mode-locked Nd:YLF laser (Coherent, Antares 76) is used to generate second harmonic radiation from LBO (527 nm) by nonlinear optics. The 527-nm radiation is used to pump three, independently controlled dye lasers (Coherent, model 700). Each dye laser is equipped with a cavity dumper (Coherent, models 7210 and 7220), three of which are synchronized to the 76-MHz signal of the Nd:YLF mode locker. The entire laser system is operated at a 400-kHz repetition rate in order to match the flow properties of the liquid BR sample jet. The velocity of the BR sample in the 400 μm square nozzle is adjusted to 12 m/s (laminar flow) to ensure a complete replacement of the sample volume between the arrival of sets

of laser pulses. Critical to this adjustment is the beam waist of the pump beam (20 μm) and the 400-kHz repetition rate of the dye lasers.

PTR/CARS signals are generated simultaneously from two separate sample compartments, reference and BR. The reference compartment is a capillary containing a static water sample placed next to the nozzle through which the BR sample flows. This parallel configuration permits the simultaneous measurement of the nonresonant background from water[29] and the PTR/CARS signal from BR, thereby minimizing the effects of any variability in the spectral intensity of the laser pulses or in the flow dynamics of the BR sample. The two sets of probe laser pulses required for these measurements are produced by amplitude division of the dye laser output by using a pellicle beam splitter. Each pair of probe laser pulses is focused separately into the reference and sample compartments using the same microscope objective ($f = 5$ cm). The signals from both compartments are collimated and focused onto the entrance slit of a triple monochromator (Spex, Triplemate). The wavelength-dispersed PTR/CARS signals are focused onto two separate, parallel stripes of a liquid nitrogen cooled, CCD multichannel array (Princeton Instruments LN/CCD-1024-F/1 UV). The spectral resolution of these CARS measurement, determined primarily by the bandwidth of the ω_1 laser,[27] is <2 cm^{-1}.

The BR photocycle is initiated via picosecond pulsed excitation (570 nm, <3 ps laser pulse, 3 nJ/pulse). The excitation conditions are selected to minimize any secondary photochemistry involving BR photocycle intermediates.[12] The probe laser wavelengths ($\omega_1 = 663$ nm and $\omega_s = 695-750$ nm) are selected to be on the low-energy (red) side of both the absorption band for BR-570 (570-nm maximum with a 50-nm bandwidth) and the photocycle intermediates under examination here (i.e., J-625, Figure 1). Since the spectral region in which the CARS signal ($\omega_a = \omega_1 + (\omega_1 - \omega_s)$) appears (542−577 nm) is about 90 nm to the red of the one-photon absorption maximum of BR-570, the major resonance enhancement can be attributed to the one-photon transition at ω_a.

The temporal synchronization of the laser pulses, monitored throughout each PTR/CARS experiment with an autocorrelator (FR-103XL, Femtochrome Research, Inc.), is characterized by a CCT for the two probe laser pulses of ~8 ps. The temporal pulse widths for ω_1 and ω_s are 5.5 and 7 ps, respectively (assuming Gaussian pulse envelopes). The timing jitter between the excitation pulse (ω_1) and the two probe pulses (ω_1 and ω_s) is measured to be <2 ps. The picosecond timing sequences and delays among the three dye laser pulses are selected by three separate, but correlated optical delay lines.[27]

Procedurally, PTR/CARS spectra from BR samples are recorded for specific time delays between ω_p and (ω_1/ω_s). In this examination of J-625, PTR/CARS spectra are recorded at −10 ps (i.e., (ω_1/ω_s) arriving at the sample 10 ps *before* ω_p) and during the CCT. To obtain the quantitative comparisons of vibrational data from BR-570, J-625, and K-590, PTR/CARS spectra are recorded from all three BR species under the same experimental conditions (e.g., excitation wavelengths).

C. Analysis. The third-order, nonlinear susceptibility ($\chi^{(3)}$) properties of the sample that produce the CARS signal obey energy and phase-matching conditions that are described in detail elsewhere.[29] The resultant CARS signal is generated primarily during the time interval defined by the temporal width of the third-order, cross-correlation function defined by the laser pulse widths (Figure 1). This function describes the relative intensity of the CARS signal by modeling the modulus of the third-order susceptibility. Since analyses of both the BR photocycle kinetics (Figure 1) and the PTR/CARS spectrum at 0 ps (Figures 2 and 3) demonstrate that the contribution of K-590 is negligible ($<5\%$), the CARS spectra presented here can be analyzed in terms of BR-570 and J-625.

The CARS signal is essentially a sum of three terms:

$$\chi^{(3)} = \chi^{(3)}_{nr} + \chi^{(3)}_{er} + \chi^{(3)}_{vr}$$

$$= \chi^{(3)}_{nr-w} + \chi^{(3)}_{nr-o} + \chi^{(3)}_{er1} + \chi^{(3)}_{er2} + \chi^{(3)}_{vr1} + \chi^{(3)}_{vr2}$$

where $\chi^{(3)}_{nr}$ represents nonresonant CARS ($\chi^{(3)}_{nr-w}$ from the water and $\chi^{(3)}_{nr-o}$ from the opsin) and $\chi^{(3)}_{er}$ and $\chi^{(3)}_{vr}$ respectively represent electronic and vibrational resonances from the two different BR species (in this case, index 1 denotes BR-570 and index 2 denotes J-625). The background-free CARS spectra are calculated by using the parameters obtained from the nonlinear fit to the CARS signal followed by a recalculation of the function (eq 1 in ref 27).

Results

A. Resonance Enhancement and Timing. The ω_1 and ω_s probe wavelengths are selected primarily to resonantly enhance the CARS signal from J-625. The extensive spectral overlap of the BR-570 and K-590 absorption spectra (Figure 1), however, ensures that resonantly enhanced CARS signals from BR-570 and K-590 also could appear in a given PTR/CARS spectrum, depending on the time delay and the reaction kinetics describing the time-dependent concentrations of I-460, J-625, and K-590 (Figure 1B). For example, the PTR/CARS spectrum at a 50-ps delay contains signals from only BR-570 and K-590, but no contribution from J-625. Even though the ω_1 and ω_s probe wavelengths strongly overlap the J-625 absorption spectrum, its population is zero at 50 ps. Thus, both ω_1 and ω_s probe wavelengths and timing must be considered simultaneously. The rapidity with which the relative J-625 and K-590 populations change within the CCT (BR-570 concentration remains largely unchanged following excitation) dictates that their respective contributions can be separated only by a quantitative analysis of the timing used to record PTR/CARS data. These timing parameters are independent of the wavelength considerations, *vide supra*.

The time evolution of the vibrational features originating from the reactive mixture of BR-570, J-625, and K-590 can be monitored directly from PTR/CARS spectra recorded at selected time delays. These PTR/CARS spectra are presented in Figures 3 and 4 for the 800−1300 cm^{-1} and 1200−1750 cm^{-1} regions, respectively. The excitation wavelengths (i.e., resonance enhancement) and relative timing between the ω_p, ω_1, and ω_s pulses used to record these PTR/CARS data are selected to distinguish the separate contributions of BR-570, J-625, and K-590 and, thereby, to simplify the $\chi^{(3)}$ analysis.

The overall timing accuracy between ω_p and the ω_1 and ω_s probe pulses can be established by comparing the ground state BR-570 and the −10 ps PTR/CARS spectra. Since these two vibrational spectra are identical, it can be determined that the absolute timing accuracy in these PTR/CARS is <3 ps. This result is consistent with the measured CCT and autocorrelation times (ACT) used to measure the ω_1 and ω_s pulse widths (5.5 and 7 ps, respectively) and with the velocity of the BR sample jet and focus volume of the laser beams within it which are selected to ensure a complete replacement of the sample volume between sets of pump and CARS laser pulses. The ACT values

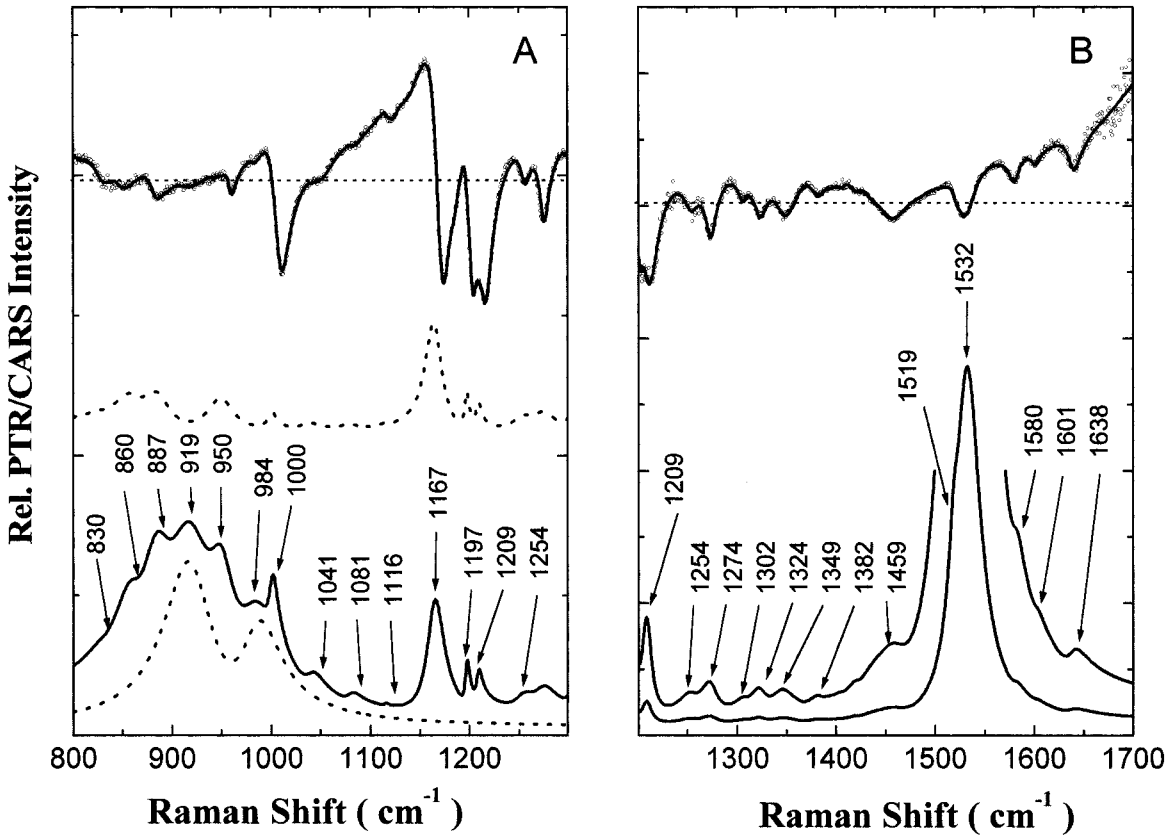

Figure 2. (A) PTR/CARS spectrum in the 800 cm^{-1} to 1300 cm^{-1} region for the reaction mixture containing BR-570 and J-625 (~38% relative concentration) taken at 0 ps after 3 ps, 570 nm excitation of BR-570. The $\chi^{(3)}$ fit function is shown as a solid line overlapping the PTR/CARS data (○). The corresponding vibrational spectrum of J-625, derived from the $\chi^{(3)}$ fit removing the nonresonant background and using Lorentzian line shape functions, is shown at the bottom (solid line). The large, broad (>200 cm^{-1}) band feature in the J-625 spectrum can be schematically approximated by two bands centered at 919 and 984 cm^{-1} (dashed line, bottom). Following the extraction of the 919 and 984 cm^{-1} features, a second J-625 spectrum (dashed line, center) is obtained. (B) PTR/CARS spectrum in the 1200 cm^{-1} to 1700 cm^{-1} region of the reaction mixture containing BR-570 and J-625 (~38% relative concentration) taken at 0 ps after 3 ps, 570-nm excitation of BR-570. The $\chi^{(3)}$ fit function is shown as a solid line overlapping the PTR/CARS data (○). The corresponding vibrational spectrum of J-625, derived from the $\chi^{(3)}$ fit removing the nonresonant background and using Lorentzian line shape functions, is shown at the bottom. Some sections of the J-625 vibrational spectrum are presented at an expanded (×6) scale.

independently establish the timing jitter between ω_p, ω_1, and ω_s pulses at <2 ps.

1. J-625 Population. The optimum temporal conditions for measuring the vibrational spectrum of J-625, given <3 ps time resolution and <2 ps jitter, can be determined from an analysis of their respective time-dependent populations based on kinetic parameters. Both J-625 and K-590 are known from transient absorption spectroscopy to be formed within the initial 10 ps of the BR photocycle: (i) J-625 forms with an ~500 fs time constant and decays to K-590 with an ~3.5 ps time constant[4,5,7,12] and (ii) K-590 decays with a >500 ps time constant.[4,7] Thus, J-625 is not present in any time-resolved spectroscopic signal (including PTR/CARS data) recorded at time delays longer than 5 ps while the concentration of K-590 becomes significant on the same time scale. The optimum time to observe J-625 by PTR/CARS (under these experimental conditions), therefore, is at 0-ps delay (during CCT) when the J-625 concentration is approaching a maximum and the K-590 concentration is not yet substantial.

2. BR-570 Contribution. To accurately determine the BR-570 contribution to PTR/CARS spectra, a CARS spectrum of BR-570 recorded under with the same degree of resonance enhancement as that used for the PTR/CARS measurement must be used. The ω_1 and ω_s probe wavelengths used to record the previously reported CARS spectrum of ground-state BR-570[30] differ from those used here, and therefore a new PR/CARS spectrum of BR-570 ($\omega_1 = 663$ nm and $\omega_s = 700-747$ nm) is presented in Figures 3 and 4 for the analysis of PTR/CARS data.

3. Relative K-590 contribution during CCT. An accurate vibrational spectrum of J-625 can be obtained from the 0-ps (CCT) PTR/CARS data only after the contribution of K-590 is quantitatively determined. This can be achieved in several different ways:

a. The relative K-590 population can be calculated from the laser power and wavelengths used to excite BR-570, the CCT and jitter times, the formation and decay kinetics of J-625 and K-590, and the quantum efficiency of the J-625/K-590 conversion (0.67).[12] For the experimental parameters used here (*vide supra*), 38% of BR-570 is optically converted into the photocycle by 570-nm excitation (3 nJ/pulse) which yields a 25% (38%X 0.67) relative K-590 concentration. This is in agreement with the results of PTA measurements.[12]

b. The time interval over which a CARS signal is generated is determined by the third-order, cross-correlation function describing the nonlinear scattering ($\langle I_1^2 I_s \rangle$) which has a shorter duration than the CCT defined by the ω_1 and ω_s probe pulses (Figure 1). Thus, in addition to their respective populations and absorption coefficients, this $\langle I_1^2 I_s \rangle$ function must be quantitatively considered when determining the relative contributions of K-590 and J-625 to the measured CARS signal.

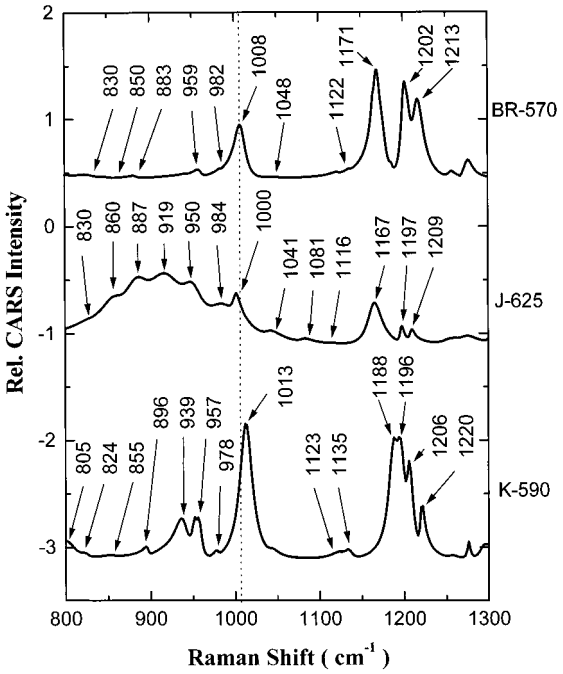

Figure 3. Background-free (Lorentzian line shape) vibrational spectra of BR-570 (top, this work), J-625 (center, this work), and K-590 (bottom)[12] in the 800−1300 cm^{-1} region. The wavenumber positions of selected bands are also presented.

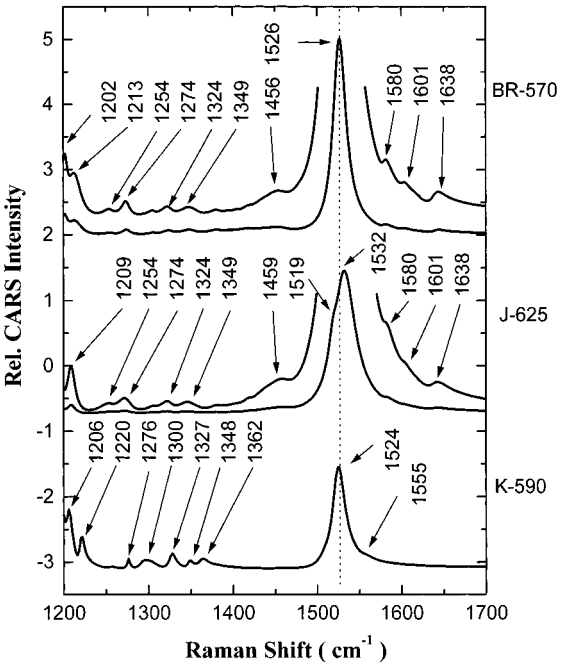

Figure 4. Background-free (Lorentzian line shape) vibrational spectra of BR-570 (top, this work), J-625 (center, this work), and K-590 (bottom)[12] in the 1200−1700 cm^{-1} region. The wavenumber positions of selected bands are also presented.

Schematic representations of the J-625 and K-590 populations relative to the temporal profiles of the ω_p pump pulse and the ω_1/ω_s CCT are shown in Figure 1B. When the schematic representation of the $\langle I_1^2 I_s \rangle$ function (Figure 1B) is compared with the K-590 population, it is evident that the K-590 contribution to the overall PTR/CARS spectrum is small (<5%). This value corresponds well with both the calculated and experimental PTA results, *vide supra*. This <5% contribution would be further reduced if either or both the lower absorption coefficient at ω_1 (Figure 1) of K-590 relative to J-625 (i.e., smaller degree of resonance enhancement) and/or the reduction in K-590 population caused by photoinduced back-reactions originating from K-590[31] are considered.

Thus, the PTR/CARS(CCT) data can be analyzed in terms of BR-570 and J-625 only. The $\chi^{(3)}$ fits to the PTR/CARS(CCT) spectrum (top) together with the resultant (background-free, Lorentizan line shape) spectra (bottom) assignable only to J-625 are shown in Figure 2. The origin positions of significant vibrational features are also presented.

Support for the conclusion that K-590 contributes little to the PTR/CARS(CCT) spectrum is found in a vibrational analysis of the J-625 CARS spectrum relative to the CARS spectrum assigned previously to K-590. These spectra together with the CARS spectrum of BR-570 are presented in Figures 3 and 4 to facilitate comparisons.

(i) The distinctive set of K-590 bands appearing in the C−C stretching (fingerprint) region which have been used to identify the 13-*cis* retinal configuration[12,32,33] are absent in the PTR/CARS (CCT) spectrum. On the contrary, the fingerprint band pattern observed is distinctly all-*trans* retinal although their individual frequencies are 2−5 cm^{-1} lower than those observed for BR-570.[34] There is no indication of a 13-*cis* band pattern as found in the PTR/CARS data from K-590.[12]

(ii) The 1220-cm^{-1} band in K-590 is not found in the PTR/CARS (CCT) data, thereby showing the absence of K-590.

(iii) The absolute frequency positions of the strong C═C stretching bands have consistently been measured to be different for BR-570 (1526 cm^{-1}) and K-590 (1524 cm^{-1}).[12] Thus, a 2-cm^{-1} decrease in C═C stretching frequency signals the formation of K-590. The 1524 cm^{-1}(K-590) band is completely absent in the PTR/CARS(CCT) spectrum. Rather, a strong C═C stretching band appears at 1532 cm^{-1} and has a shoulder at 1519 cm^{-1} (Figure 2). The 6-cm^{-1} increase in C═C stretching frequency clearly cannot be assigned to K-590.

(iv) Although the 1013-cm^{-1} band from K-590 is not present in the PTR/CARS (CCT) spectrum, a small 1000-cm^{-1} band does appear (Figure 2). The 1008-cm^{-1} band from BR-570 also changes significantly (i.e., decreases in frequency to 1000 cm^{-1} and in relative intensity by a factor of 3).

(v) The strong HOOP bands in the K-590 (957 cm^{-1} and 939 cm^{-1}) spectrum are not present in the PTR/CARS (CCT) data (Figure 2). Rather, a strong, broad HOOP vibrational feature is present in the PTR/CARS (CCT) spectrum and is not found in either the BR-570 and K-590 vibrational spectra.

Thus, both the kinetic and vibrational analyses lead to the conclusion that the contribution made by K-590 to the PTR/CARS(CCT) spectrum is extremely small. The PTR/CARS-(CCT) spectrum obtained by the extraction of the BR-570 contribution (following the $\chi^{(3)}$ fitting process), therefore, can be assigned to J-625 alone (Figure 2).

B. CARS Spectrum of J-625. *1. C═C Stretching and Schiff Base Region (1500−1650 cm^{-1}).* The dominate 1532-cm^{-1} feature has a relatively broad bandwidth (30 cm^{-1} (fwhm)) which contains a shoulder at 1519 cm^{-1}. Although qualitatively similar to the 1526-cm^{-1} band observed in BR-570,[12,35,36] the 1532-cm^{-1} feature in J-625 represents an unusual frequency increase in the C═C stretching mode. Given the large red-shift (relative to that of BR-570) of the J-625 absorption band, the increased C═C stretching frequency is opposite to that predicted by a π-electron delocalization model.[34,37] The C═C stretching frequencies assigned to other BR intermediates (e.g., K-590) appear to follow this model.

The other, less intense bands at 1580, 1601, and 1638 cm^{-1} are essentially the same as those in BR-570 and J-625. The

absence of change in the 1638-cm band suggests that the Schiff base bonding in BR-570 and J-625 are essentially the same.

2. C−C Stretching (1050−1300 cm^{-1}). Three prominent bands, at 1167, 1197, and 1209 cm^{-1}, appear in the spectral region assigned to modes primarily involving C−C stretching character (some C−H in-plane rocking modes also). This band pattern is similar to that found for BR-570 (1171, 1202, and 1213 cm^{-1}),[30] although in J-625 all three band frequencies decrease. Their relative intensities also differ.

3. HOOP Region (800−1000 cm^{-1}). (a) The HOOP region is dominated by a large, broad (200-cm^{-1} wide) feature which underlies narrow vibrational bands at 830, 860, 887, 950, 919, and 984 cm^{-1} (Figure 2). Although HOOP vibrations assignable to twists/distortions around the C═C and C−C polyene bonds are found in the vibrational spectra of most BR intermediates, nothing analogous to this 200-cm^{-1} vibrational feature has been reported previously. The PTR/CARS (CCT) data cannot be fit well in a $\chi^{(3)}$ analysis without this 200-cm^{-1} feature.

(b) The prominent 1008-cm^{-1} band (assigned to the in-plane CH_3-rocking mode) observed in the BR-570 spectrum is not present, although a small band at 1000 cm^{-1} does appear.

(c) The relationships between these six, relatively narrow HOOP bands and the analogous BR-570 and K-590 bands are important to establish. These relationships can be evaluated more easily if the broad 200-cm^{-1} HOOP feature is artificially removed by calculating a quantitative fit to two broad bands centered at 919 cm^{-1} and 984 cm^{-1} (shown as dashed lines in Figure 2). Once the 200-cm^{-1} feature is schematically removed, a CARS spectrum (presented in the middle of Figure 2) containing clearly defined bands at 830, 860, 887, 950, 919, 984, and 1000 cm^{-1} is obtained. All of these bands are assignable to J-625.

Discussion

A. Vibrational Assignments in the J-625 Spectrum. Comparisons of the CARS spectra of BR-570, J-625, and K-590 show that time-dependent differences in the respective vibrational bands are found in essentially all spectral regions. Such comparisons provide a basis for assigning vibrational modes to specific bands in the J-625 spectrum. To facilitate these comparisons, the background-free, Lorentzian CARS spectra (obtained by $\chi^{(3)}$ analysis) of BR-570, J-625, and K-590 are presented together in Figures 3 and 4.

1. C═C Stretching and Schiff Base Regions. The vibrational band patterns in the C═C stretching and Schiff base region for BR-570 and J-625 are similar (Figure 4). The Schiff base mode in J-625 appears at the same position (1638 cm^{-1}) as in BR-570 which indicates that the C═NH linkage between the retinal chromophore and lysine of the protein is the same.

The frequency of the most intense BR-570 band at 1526 cm^{-1}, assigned primarily to the symmetric combination of the C_9═C_{10} and C_{11}═C_{12} stretching modes with a small contribution from C_7═C_8 and C_{13}═C_{14} stretching modes,[34,37] increases in J-625 to 1532 cm^{-1} with a shoulder at 1519 cm^{-1}. The frequency of the analogous band in K-590 decreases to 1524 cm^{-1} and has an intensity which is 10 times smaller than respective bands in BR-570 and J-625 (Figure 4).[12]

The less intense BR-570 bands, appearing as shoulders at 1580 cm^{-1} and 1601 cm^{-1} and assigned to the C_{13}═C_{14} and C_7═C_8 stretching modes with small contributions from the C_5═C_6 stretching mode,[37] appear at the same positions in the J-625 spectrum.

The vibrational assignments of the 1532-cm^{-1} and 1519-cm^{-1} bands in J-625 can be derived from a consideration of the symmetric and antisymmetric components that separate by twisting of the polyene chain. These two components appear as a single band at 1526 cm^{-1} in BR-570.[12,35] By analogy with the calculated 1533-cm^{-1} band in BR-570,[37] the 1532-cm^{-1} band in J-625 can be assigned to the antisymmetric combination of the C_9═C_{10} and C_{11}═C_{12} stretching modes. The appearance of the 1532-cm^{-1} band indicates that twisting along the polyene chain activates the antisymmetric modes with respect to Raman scattering. The small 1519-cm^{-1} band, therefore, can be associated with the antisymmetric combination of the C_7═C_8 and C_{13}═C_{14} modes which contributes only slightly to the 1526-cm^{-1} band observed in the BR-570 spectrum.

In the K-590 CARS spectrum,[12] the primary C═C stretching band appears at 1524 cm^{-1} which is 8 cm^{-1} lower than the analogous J-625 band (Figure 4). In addition, the band narrows and has only a small shoulder at 1555 cm^{-1}. The 1580-cm^{-1} and 1601-cm^{-1} bands, assigned in BR-570 to the C_{13}═C_{14} and C_7═C_8 stretching modes, remain at the same frequencies in J-625, but have diminished intensities. These changes in the K-590 spectrum (relative to J-625) reflect a more, though not completely, relaxed (i.e., planar) polyene chain which has assumed a different (13-*cis*) retinal configuration.

2. C−C Stretching Region. The general pattern of vibrational bands in the fingerprint region of J-625 is the same as that found in the BR-570 spectrum,[12,36,38] thereby suggesting that the retinal remains largely in an all-*trans* configuration. This conclusion is supported by the observation that the corresponding fingerprint pattern of bands in the K-590 spectrum is completely different, thus reflecting a 13-*cis* retinal configuration.[12,39,40] These vibrational data show that J-625 has a primarily all-*trans* retinal configuration, thereby demonstrating that C_{13}═C_{14} isomerization occurs as J-625 transforms into K-590 and not before.

The frequencies of the three C−C stretching bands in J-625 (at 1166, 1197, and 1209 cm^{-1}) decrease relative to the respective BR-570 bands (at 1171, 1202, and 1213 cm^{-1}). Based on the respective assignments of these BR-570 bands to the C_{10}−C_{11}, C_{14}−C_{15}, and C_8−C_9 stretching modes,[37] the J-625 bands are assigned to the analogous modes. Thus, the decreases of these frequencies, together with the frequency increases observed in the J-625 C═C stretching bands (*vide supra*), show that electron delocalization along the polyene chain changes significantly when J-625 is formed from BR-570, thereby resulting in a general increase of the C═C bond order and a decrease in the C−C bond order.

The frequencies of the lower intensity bands at 1274 cm^{-1}, 1324 cm^{-1}, and 1349 cm^{-1} do not change when J-625 appears. The absence of changes in the 1254 cm^{-1} band frequency in J-625, assigned in BR-570 to the C_{12}−C_{13} stretching mode,[34] is of special interest since its frequency does decrease to 1220 cm^{-1} in K-590.[12] This frequency decrease is attributed to twisting of the polyene chain during the early (<500 ps) lifetime of K-590.[8,12,40] The absence of such a frequency change in J-625, together with the frequency changes assigned to the C_{13}═C_{14} stretching mode (*vide supra*), demonstrates that the retinal in J-625 does not significantly twist/distort around the C_{12}−C_{13}═C_{14} bonds.

3. C−CH_3 Rocking. The intense 1008-cm^{-1} band appearing in the BR-570 spectrum (assigned primarily to symmetric, in-plane C−CH_3 rocking modes located at C_9 and C_{13}[37]) is not observed in the J-625 spectrum, but rather, a low intensity 1000-cm^{-1} band is present (Figure 2). In K-590, neither the 1008-cm^{-1} nor 1000-cm^{-1} band appears, but rather a strong band at 1013 cm^{-1} is found (Figure 3). These shifting band frequencies and varying intensities suggest that these methyl groups (C_9−

$C_{19}H_3$ and $C_{13}-C_{20}H_3$) have changing degrees of in-plane flexibility as BR-570 transforms into J-625 and subsequently into K-590. Changing in-plane motions may be associated with the interactions (e.g., steric hindrance) between these methyl groups and specific amino acids comprising the retinal binding pocket. Thus, the freely moving methyl group(s) found in BR-570 become transiently restricted in J-625 before becoming free again in K-590.

The restricted (e.g., blocked) in-plane methyl rocking motion in J-625 may be associated with strain introduced into the retinal by the twisting of the polyene chain (*vide supra*). The PTR/CARS spectrum of J-625 clearly shows significant out-of-plane, retinal distortion that is distinct from that found in K-590 (Figure 2). The HOOP motion observed in the K-590 formed within picoseconds of BR excitation relaxes within a nanosecond.[11,41−43]

Vibrational mode assignments reported previously for BR-570[34,37,39] suggest that the in-plane $C_9-C_{19}H_3$ rocking mode is primarily responsible for the 1008-cm^{-1} band in BR-570 which changes dramatically upon J-625 formation. This assignment is supported by the observation that the weak 1048-cm^{-1} band, assigned to the out-of-plane $C_9-C_{19}H_3$ rocking mode in BR-570, decreases to 1041 cm^{-1} in J-625. The changes in the C=C and C−C stretching frequencies (*vide infra*) independently suggest that $C_9-C_{19}H_3$ is more flexible than the $C_{13}-C_{20}H_3$ and, therefore, that the 1008-cm^{-1} band is primarily due to the former. The asymmetric deformations of the methyl groups, appearing at 1456 cm^{-1} in BR-570, at 1459 cm^{-1} in J-625, and at 1450 cm^{-1} in K-590, are assigned primarily to $C_{13}-C_{20}H_3$ due to its relative rigidity.[37]

4. HOOP Region. The relatively strong intensities and broad band nature of the 919 cm^{-1} ($\Delta\nu$ ~31 cm^{-1}) and 984 cm^{-1} ($\Delta\nu$ ~25 cm^{-1}) HOOP bands in the CARS spectrum of J-625 (dashed line in Figure 2) clearly indicate that the polyene chain contains a significant amount of out-of-plane motion and may have a twisted/distorted retinal structure. The extremely broad (200 cm^{-1}) nature of the overall feature is highly unusual having no analogous feature reported previously for a BR species. Such breadth suggests that a large amount of delocalized, out-of-plane motion is present which is not assignable to specific normal modes, but which is rather distributed widely throughout the retinal structure. The disappearance of this broad feature when K-590 is formed signals a localization of the out-of-plane motion into well-defined normal modes which persist throughout the remainder of the BR photocycle.

The 984-cm^{-1} band, which has a low intensity counterpart at 982 cm^{-1} in BR-570, can be assigned to the C_7H and C_8H wagging modes. The 919-cm^{-1} band, though having no counterpart in BR-570, can be tentatively assigned to the harmonic vibrations of several out-of-plane motions. Its presence indicates that nonlocalized hydrogen out-of-plane wagging occurs. Other bands at 860, 887, and 950 cm^{-1} can be associated with the analogous BR-570 bands at 850, 883, and 959 cm^{-1}, respectively.

B. Structure of J-625. When compared with CARS spectra of BR-570 and K-590, the PTR/CARS vibrational spectrum of J-625 presented here provides new insight into the changes in structure and π-electron delocalization underlying the femto/picosecond molecular events that comprise the room-temperature BR photocycle.

1. C=C Stretching Frequency. As the strongest feature in the Raman spectra of BR species, the frequency position of the C=C stretching band, $\omega_{C=C}$ (assigned to several modes), has been used repeatedly to characterize π-electron delocalization within the retinal chromophore as well as the retinal structure

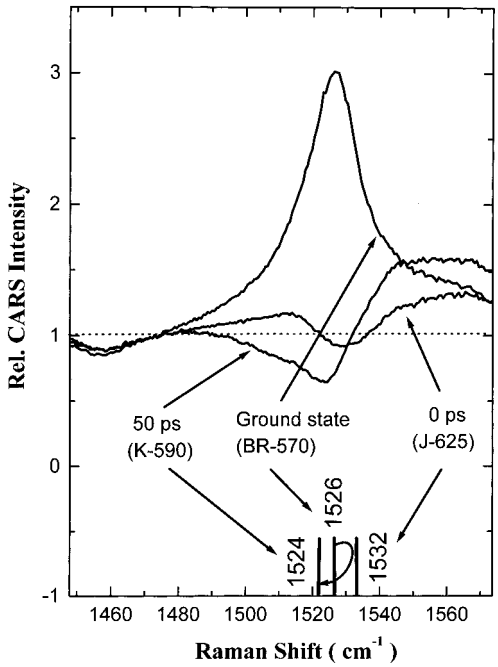

Figure 5. Picosecond resonance CARS spectrum of native BR-570 (ground state) and PTR/CARS spectra recorded at 0 ps (J-625) and 50 ps (K-590) time delays in the 1460−1570 cm^{-1} region (horizontal dashed line is nonresonant CARS background signal from water). These CARS spectra show the time evolution of the 1527 cm^{-1} band assigned to BR-570, the 1532 cm^{-1} band assigned to J-625, and the 1524 cm^{-1} band assigned to K-590 over the 0−50 ps interval of the BR photocycle. The 0-ps data mainly contain mixtures of intermediate J-625 and ground state BR-570 while the 50-ps data mainly contain mixtures of intermediate K-590 and ground state BR-570.

itself.[34] The appearance of $\omega_{C=C}$ larger than the 1526-cm^{-1} value assigned to BR-570, however, is unexpected in view of the widely accepted model relating absorption maximum with $\omega_{C=C}$[4,7,8] (i.e., the red-shifted absorption maximum of J-625 relative to BR-570 (and K-590) would predict $\omega_{C=C}$ < 1526 (<1524) cm^{-1}). Its actual position at 1532 cm^{-1}, therefore, reflects a change in the π-electron delocalization properties of the retinal that distinguishes J-625 from BR-570 and K-590. A larger $\omega_{C=C}$ value, however, does agree with an earlier reported $\omega_{C=C}$ = 1575 cm^{-1} obtained by 1-ps excitation of BR which is assigned to I-460 and not J-625.[16] The transient formation of J-625 can be viewed in terms of $\omega_{C=C}$ as shown in Figure 5 where the CARS data from BR-570, J-625, and K-590 are presented together with the positions of their respective $\omega_{C=C}$ values.

2. π-Electron Delocalization. The changes of $\omega_{C=C}$ and ω_{C-C} observed between BR-570, J-625, and K-590 independently reflect asymmetric shifts in the π-electron delocalization among the polyene bonds. The major change in $\omega_{C=C}$ (1526 to 1532 cm^{-1}) indicates increased π-electron density in the $C_{11}=C_{12}$ and $C_9=C_{10}$ stretching modes (assigned from resonance Raman spectra[34]). Analogously, the decreased $C_{10}-C_{11}$, $C_{14}-C_{15}$, and C_8-C_9 stretching frequencies (respectively at 1188, 1196, and 1206 cm^{-1} in K-590) reflect decreased π-electron density in these bonds. The absence of changes in the $C_{12}-C_{13}$ and $C_{13}=C_{14}$ stretching frequencies (at 1254 and 1580 cm^{-1} in J-625) indicates that the π-electron density remains the same in these bonds. Thus, relative to BR-570, the overall π-electron delocalization within retinal shifts toward the center of the polyene chain (i.e., around the $C_8-C_9=C_{10}-C_{11}=C_{12}$ bonds) when J-625 is formed even though the retinal configuration remains all-*trans*.

The changes in $\omega_{C=C}$ and ω_{C-C} between J-625 and K-590, reflecting the next stage of the BR photocycle, also indicate a shift in the π-electron delocalization within the polyene chain which accompanies the all-*trans* to 13-*cis* retinal isomerization. The major $\omega_{C=C}$ decrease (1532 to 1524 cm^{-1}) indicates decreased π-electron density in the $C_{11}=C_{12}$ and $C_9=C_{10}$ stretching modes, while the increases of the $C_{10}-C_{11}$, $C_{14}-C_{15}$, and C_8-C_9 stretching frequencies (respectively at 1188, 1196, and 1206 cm^{-1} in K-590) reflect increased π-electron density in these bonds. The absence of changes in the $C_{12}-C_{13}$ and $C_{13}=C_{14}$ stretching frequencies (at 1254 and 1580 cm^{-1} in J-625) indicates that the π-electron density in these bonds remains the same. Thus, relative to J-625, the overall π-electron delocalization within retinal shifts away from the center of the polyene chain (i.e., toward the $C_8-C_9=C_{10}-C_{11}$ and $C_{14}=C_{15}$ bonds) when K-590 is formed. These π-electron density changes are accompanied by the all-*trans* to 13-*cis* isomerization of retinal.

3. Retinal Configuration. PTR/CARS data from the C−C stretching region demonstrate that while the retinal configurations in J-625 and K-590 are completely different, those of J-625 and BR-570 are similar. Comparisons of CARS spectra (Figure 3) show that the general C−C stretching band patterns are the same for BR-570 and J-625 while both differ significantly from that found for K-590 (assigned as 13-*cis* retinal[12,34]). Although the C−C stretching frequencies decrease as J-625 is formed from BR-570 (Figure 3), the all-*trans* retinal band pattern remains the same (relative band intensities do change, Figure 3). Even the presence of significant delocalized, out-of-plane motion in J-625 (*vide supra*) does not appear to alter the all-*trans* retinal backbone of J-625. By contrast, the C−C stretching band patterns of J-625 and K-590 are completely different (Figure 3). Thus, these C−C stretching band data show that the *trans* to *cis* isomerization around the $C_{13}=C_{14}$ bond in BR occurs only during the J-625 to K-590 transformation.

4. Schiff Base Bonding. The observation that the 1638-cm^{-1} and 1349-cm^{-1} bands (assigned to the C=N stretching and N−H in-plane rocking modes, respectively) do not change upon the formation of J-625 indicates that the Schiff base bonding environment (including the role of water molecules bound at C=NH and/or any retinal protein interactions) remains essentially the same in BR-570 and J-625. Since no band assignable to the C=N stretching mode has been reported for K-590, there is a dramatic change in the Schiff base bonding as J-625 transforms into K-590. These observations support the conclusion that $C_{13}=C_{14}$ isomerization does not occur between BR-570 and J-625, but rather between J-625 and K-590.

5. Methyl In-Plane Rocking Motion. The changes of the $C_{19}-CH_3$ rocking motion when J-625 appears indicates that there exists a transient interaction between the CH_3 rocking mode of the retinal and the surrounding amino acid(s) comprising the binding pocket (i.e., tryptophan 182 of helix F[44]). Although the precise driving force that initiates the CH_3 rocking/amino acid interaction remains to be determined, it may be associated with the polyene chain twisting/distortion reflected in the changes in π-electron delocalization around the $C_8-C_9=C_{10}-C_{11}=C_{12}$ bonds (*vide supra*). Such twisting/distortion could be anticipated to displace the $C_{19}-CH_3$ bond away from the retinal toward the amino acids comprising the binding pocket, thereby altering/blocking the $C_{19}-CH_3$ rocking motion and decreasing the intensity of the 1008-cm^{-1} band of BR-570 (Figure 3). If the $C_{19}-CH_3$ bond displacement is associated with the twisting/distortion of the polyene chain around the $C_8-C_9=C_{10}-C_{11}=C_{12}$ bonds (*vide supra*), then the retinal/amino acid interaction could also halt this twisting/distortion. The disappearance of the $C_{19}-CH_3$ rocking/amino acid interaction may also signal the increased flexibility in the $C_{13}=C_{14}$ bond that is a prerequisite for $C_{13}=C_{14}$ *trans* to *cis* isomerization and the formation of K-590. This mechanism would also affect the transfer of energy stored in the torsional strain of polyene chain into retinal isomerization.

The appearance of the intense 1013-cm^{-1} band in K-590 (Figure 3) demonstrates that a relatively relaxed polyene chain can be obtained which includes a freely moving $C_{19}-CH_3$ rocking mode without interactions with the amino acid binding pocket.

6. Hydrogen Out-of-Plane (Hoop) Motion. Since HOOP wagging modes are expected to have little or no intensity in the CARS spectrum of a planar retinal chromophore, the appearance of intense, broad band HOOP features in the J-625 PTR/CARS spectrum (Figure 3) supports the existence of significant torsional motion within the polyene chain and a nonplanar retinal structure in J-625. Previous studies of resonance Raman intensities have shown that bands assignable to out-of-plane motions have enhanced intensities when the chromophore is torsionally distorted.[34,37]

One of the most distinctive aspects of the J-625 vibrational spectrum is the large, broad spectral feature in the 850−1050 cm^{-1} region assignable to HOOP motions and uniquely observed in J-625 (Figure 3). The HOOP features appearing in the vibrational spectra of other BR species (ground state and intermediates) can have significant intensities, but all have relatively narrow bandwidths which can be assigned to specific, *localized* normal vibrational modes.[33,34] By contrast, this broad 200-cm^{-1} J-625 feature appears to represent another type of vibrational degree of freedom involving *delocalized* HOOP motions in the retinal chromophore that are not readily described by a specific normal vibrational mode. Such delocalized HOOP motion appears throughout the retinal and is time dependent since, as the photocycle proceeds, it becomes localized within well-defined normal modes as manifested by the appearance of narrow, less intense vibrational bands (e.g., in K-590).

These broad features can be approximated by two adjacent bands (centered at 919 and 984 cm^{-1}) which can be schematically removed from the PTR/CARS spectrum to produce a vibrational CARS spectrum comparable to others measured for BR intermediates (Figure 2). Like the 850−1050-cm^{-1} feature, these specific smaller HOOP bands are not present in the K-590 PTR/CARS spectrum (Figure 3).

The short time scale on which this 200-cm^{-1} feature appears (<500 fs) and disappears (not found in K-590 at 3.5 ps, Figure 3) suggests that it results from the reorientation of the retinal associated with the energy deposited by the initial optical absorption in BR-570. Since mechanistically J-625 is formed sequentially from I-460 which is created following the population of the Franck−Condon states by optical absorption (i.e., H[46]), the delocalized HOOP vibrations observed in J-625 may be caused by the rapid (<500 fs) deposition of excited electronic state energy into a group of related reaction coordinates (i.e., HOOP modes) which favor the eventual $C_{13}=C_{14}$ isomerization. The subsequent localization of HOOP energy in K-590 suggests that such delocalized vibrational motions cannot be sustained for long (<3.5 ps). Protein−retinal interactions appear to control the localization of such vibrational energy.

The broad line shape may also reflect a short vibrational dephasing time for a more specific set of the HOOP modes that favor $C_{13}=C_{14}$ isomerization. The identification of HOOP modes as reaction coordinates is consistent with theoretical

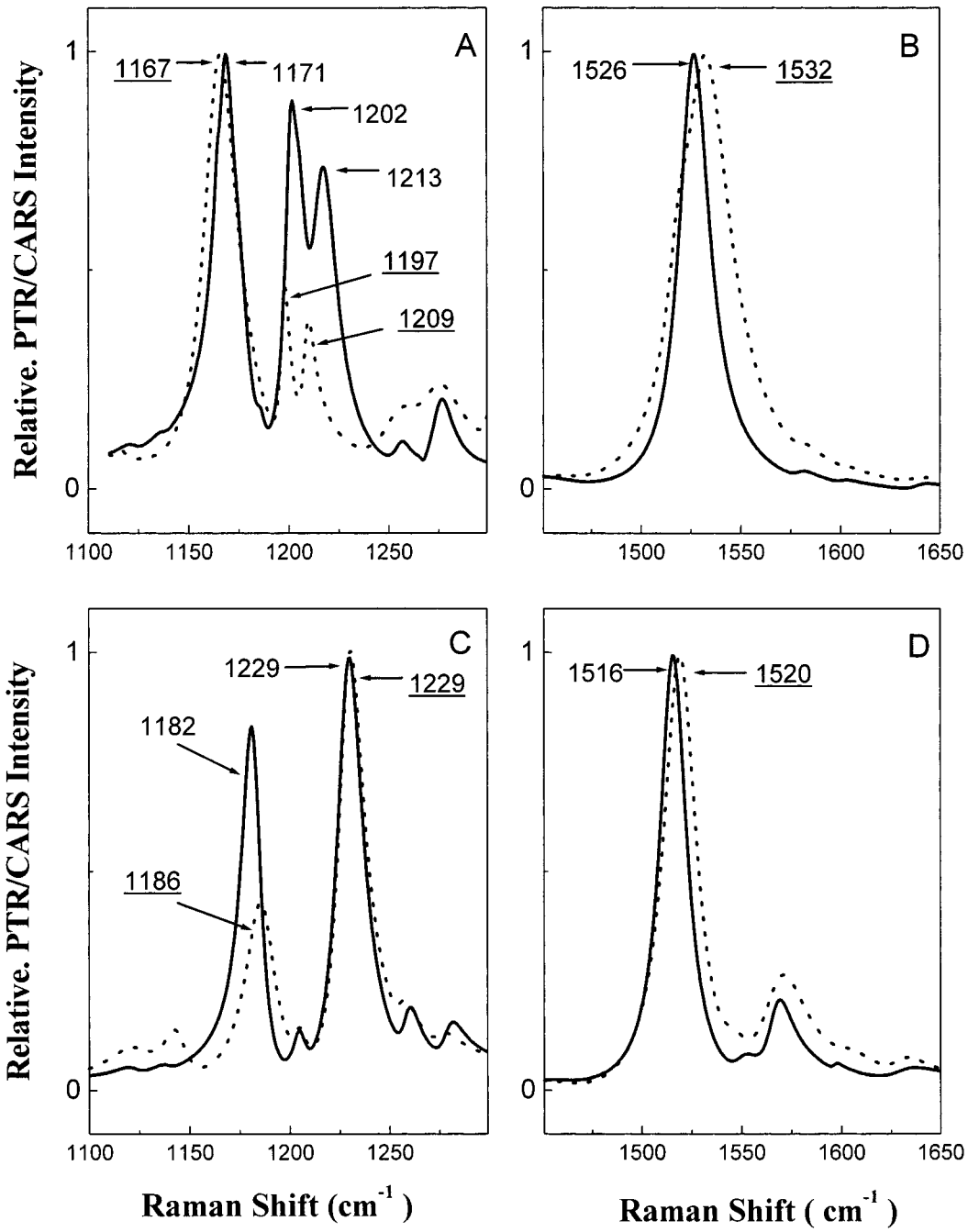

Figure 6. Comparison of the general band patterns and positions for the J-625 and T5.12 intermediates (dashed lines) relative to their respective ground state species BR-570 and BR5.12 (solid lines). The band positions for the BR-570 and J-625 (numerical values underlined) in the C−C stretching (A) and C═C stretching (B) regions and for the BR5.12 and T5.12 (numerical values underlined) in the C−C stretching (C) and C═C stretching (D) regions are presented.

models[47,48] in which coupling between the excited ^1A_g and ^1B_u electronic states is a precondition for C_{13}═C_{14} isomerization. Since such broadening is not observed in the other vibrational modes in the J-625 spectrum, HOOP modes may be the retinal coordinates which facilitate the electronic state coupling in the primary reaction mechanism of BR.

Collectively, these PTR/CARS data show that J-625 has completely different HOOP vibrations than either BR-570 or K-590 and that J-625 reflects (i) a reorganization of the π-electron density among C═C and C−C stretching modes, (ii) an all-*trans*-like retinal configuration, (iii) a Schiff base bonding similar to that in BR-570, (iii) a site-specific, transient C_{19}−CH_3/amino acid interaction which restricts the methyl rocking motion, and (iv) a large degree of delocalized out-of-plane motion reflecting a torsionally strained, nonplanar polyene chain. Mechanistically, it is shown that isomerization around the C_{13}═C_{14} bond occurs as J-625 forms K-590 and not before, although distortion at or near the C_{13}═C_{14} bond is present in J-625. This mechanism reflects the conversion of potential energy stored in the torsional strain of the polyene chain found in J-625 and it precedes *trans* to *cis* (C_{13}═C_{14}) isomerization.

Mechanistically, these PTR/CARS results show that C_{13}═C_{14} bond isomerization has not yet occurred in J-625, but rather occurs as J-625 transforms into K-590. Although no conclusion can be reached directly from these PTR/CARS data concerning whether J-625 is an excited or ground electronic state species, the all-*trans* nature of the retinal in J-625 remains unaffected. The most convincing evidence supporting a ground state

assignment for J-625 derives from the absence of any observed emission from J-625, but until a wider spectral range is examined (e.g., infrared), this negative results should be viewed with caution. It is also possible that emission (both spontaneous and stimulated) from J-625 has not been observed because it is forbidden by electronic state selection rules. In this latter case, J-625 would be an excited electronic state.

C. J-625 and the Artificial BR Intermediate, T5.12. PTA and PTR/CARS studies of the photoreaction of an artificial BR pigment containing a five-membered ring spanning the $C_{12}-C_{13}=C_{14}$ bond (BR5.12) revealed the presence of a picosecond intermediate, T5.12, which may have structural analogies to J-625.[45] With the availability of vibrational data assignable directly to J-625 from the results presented here, it is now feasible to directly compare the spectra data from T5.12 and J-625.

The PTR/CARS spectra of J-625 and T5.12 are similar, with the primary difference appearing in the HOOP region where the J-625 spectrum contains the intense 850−1050-cm^{-1} feature (Figure 2). No feature of this type appears in the vibrational spectra of any other BR species including T5.12.[45]

The absence of the 850−1050-cm^{-1} feature in T5.12 supports its assignment to delocalized, out-of-plane motion since T5.12 contains a ring structure that can be anticipated to generally restrict out-of-plane motion throughout the retinal, and especially near the $C_{12}-C_{13}=C_{14}$, bonds. Since the 850−1050-cm^{-1} feature is unique to J-625, it may represent an important component of the structural mechanism that facilitates the efficiency and/or bond specificity of the all-*trans* to 13-*cis* isomerization in the BR photocycle. The presence of the five-membered ring in BR5.12 prevents such delocalized motion from appearing in the T5.12 intermediate. In all other regards, however, the vibrational spectra of T5.12 and J-625 are analogous, showing that the two intermediates have retinal chromophores with similar vibrational degrees of freedom.

Such structural similarities can also be seen from comparisons of the major changes in the J-625 and T5.12 PTR/CARS spectra relative to those from their respective ground states, BR-570 and BR5.12. Comparisons to the respective ground states are appropriate since the introduction of a five-membered ring slightly alters the vibrational degrees of freedom (CARS spectra) in the retinal.[30] These comparison are shown in Figure 6 for the C=C and C−C stretching modes. It is evident from the C−C stretching bands that, like J-625 (*vide supra*), T5.12 preserves the same band pattern (relative intensities do change, Figures 6A and 6C) and, therefore, maintains the same retinal configuration as its ground state (all-*trans* BR5.12, no $C_{13}=C_{14}$ isomerization can occur). In addition, the value of $\omega_{C=C}$ increases for both T5.12 and J-625 (Figures 6B and 6D). These similarities between the T5.12 and J-625 vibrational spectra support the general conclusions concerning the J-625 structure drawn from the PTR/CARS presented here.

References and Notes

(1) Oesterhelt, D.; Tittor, J. *TIBS* **1989**, *14*, 57−61.

(2) Mathies, R. A.; Lin, S. W.; Ames, J. B.; Pollard, W. T. *Annu. Rev. Biophys. Biophys. Chem.* **1991**, *20*, 491−518.

(3) Honig, B.; Ebrey, T.; Callender, R. H.; Dinur, U.; Ottolenghi, M. *Proc. Natl. Acad. Sci. U.S.A.* **1979**, *76*, 2503−2507.

(4) Nuss, M. C.; Zinth, W.; Kaiser, W.; Kolling, E.; Oesterhelt, D. *Chem. Phys. Lett.* **1985**, *117*, 1−7.

(5) Polland, H.-J.; Franz, M. A.; Zinth, W.; Kaiser, W.; Kolling, E.; Oesterhelt, D. *Biophys. J.* **1986**, *49*, 651−662.

(6) Sharkov, A. V.; Pakulev, A. V.; Chekalin, S. V.; Matveetz, Y. A. *Biochim. Biophys. Acta* **1985**, *808*, 94−102.

(7) Dobler, J.; Zinth, W.; Kaiser, W.; Oesterhelt, D. *Chem. Phys. Lett.* **1988**, *144*, 215−220.

(8) Mathies, R. A.; Cruz, C. H.; Pollard, W. T.; Shank, C. V. *Science* **1988**, *243*, 777−779.

(9) Blanchard, D.; Gilmore, D. A.; Brack, T. L.; Lemaire, H.; Hughes, D.; Atkinson, G. H. *Chem. Phys.* **1991**, *156*, 155−170.

(10) Delaney, J. K.; Brack, T. L.; Atkinson, G. H. *Biophys. J.* **1993**, *64*, 1512−1519.

(11) Weidlich, O.; Ujj, L.; Jäger, F.; Atkinson, G. H. *Biophys. J.* **1997**, *72*, 2329−2341.

(12) Ujj, L.; Jäger, F.; Popp, A.; Atkinson, G. H. *Chem. Phys.* **1996**, *212*, 421−436.

(13) Braiman, M.; Mathies, R. A. *Proc. Natl. Acad. Sci. U.S.A.* **1982**, *79*, 403−407.

(14) Petrich, J. W.; Breton, J.; Martin, J. L.; Antonetti, A. *Chem. Phys. Lett.* **1987**, *137*, 369−375.

(15) Doig, S. J.; Reid, P. J.; Mathies, R. A. *Biomol. Spectrosc.* **1991**, *1432*, 184−195.

(16) Song, L.; El-Sayed, M. A. *J. Am. Chem. Soc.* **1999**, *120*, 8889−8890.

(17) Hasson, K. C.; Gai, F.; Anfinrud, P. A. *Proc. Natl. Acad. Sci. U.S.A.* **1996**, *93*, 15124−15129.

(18) Callender, R. H.; Honig, B. *Annu. Rev. Biophys. Bioeng.* **1977**, *6*, 33−55.

(19) Birge, R. R.; Findsen, L. A.; Pierce, B. M. *J. Am. Chem. Soc.* **1987**, *109*, 5041−5043.

(20) Haran, G.; Wynne, K.; Xie, A.; He, Q.; Chance, M.; Hochstrasser, R. M. *Chem. Phys. Lett.* **1996**, *261*, 389−395.

(21) Humphrey, W.; Xu, D.; Sheves, M.; Schulten, K. *J. Phys. Chem.* **1995**, *99*, 14549−14560.

(22) Zhong, Q.; Ruhman, S.; Ottolenghi, M.; Sheves, M.; Friedman, N.; Atkinson, G. H.; Delaney, J. K. *J. Am. Chem. Soc.* **1997**.

(23) Rousso, I.; Khachatryan, E.; Gat, Y.; Brodsky, I.; Ottolenghi, M.; Sheves, M.; Lewis, A. *Proc. Natl. Acad. Sci. U.S.A.* **1997**, *94*, 7937−7941.

(24) Garavelli, M.; Celani, P.; Bernardi, F.; Robb, M. A.; Olivucci, M. *J. Am. Chem. Soc.* **1997**, *119*, 6891−6901.

(25) Kamalov, V. F.; Masciangioli, T. M.; El-Sayed, M. A. *J. Phys. Chem.* **1996**, *100*, 2762−2765.

(26) Oesterhelt, D.; Stoeckenius, W. *Proc. Natl. Acad. Sci. U.S.A.* **1973**, *70*, 2853−2857.

(27) Ujj, L.; Jäger, F.; Atkinson, G. H. *Biophys. J.* **1998**, *74*, 1492−1501.

(28) Jäger, F.; Lou, J.; Nakanishi, K.; Ujj, L.; Atkinson, G. H. *J. Am. Chem. Soc.* **1998**.

(29) Ujj, L.; Volodin, B. L.; Popp, A.; Delaney, J. K.; Atkinson, G. H. *Chem. Phys.* **1994**, *182*, 291−311.

(30) Delaney, J. K.; Brack, T. L.; Atkinson, G. H.; Ottolenghi, M.; Steinberg, G.; Sheves, M. *Proc. Natl. Acad. Sci. U.S.A.* **1995**, *92*, 2101−2105.

(31) Bazhenov, V.; Schmidt, P.; Atkinson, G. H. *Biophys. J.* **1992**, *61*, 1630−1637.

(32) Harbison, G. S.; Smith, S. B.; Pardoen, J. A.; Winkel, C.; Lugtenburg, J.; Herzfeld, J.; Mathies, R. A.; Griffin, R. G. *Proc. Natl. Acad. Sci. U.S.A.* **1984**, *81*, 1706−1709.

(33) Smith, S. O.; Lugtenburg, J.; Mathies, R. A. *J. Membr. Biol.* **1985**, *85*, 95−109.

(34) Smith, S. O.; Braiman, M.; Myers, A. B.; Pardoen, J. A.; Courtin, J. M.; Winkel, C.; Lugtenburg, J.; Mathies, R. A. *J. Am. Chem. Soc.* **1987**, *109*, 3108−3125.

(35) Brack, T. L.; Atkinson, G. H. *J. Mol. Struct.* **1989**, 289−303.

(36) Atkinson, G. H.; Brack, T. L.; Blanchard, D.; Rumbles, G. *Chem. Phys.* **1989**, *131*, 1−15.

(37) Smith, S. O., Ph.D. Dissertation, 1985, pp 1−344.

(38) Brack, T. L.; Atkinson, G. H. *J. Mol. Struct.* **1989**, *214*, 289−303.

(39) Smith, S. O.; Pardoen, J. A.; Lugtenburg, J.; Mathies, R. A. *J. Phys. Chem.* **1987**, *91*, 804−819.

(40) Doig, S. J.; Reid, P. J.; Mathies, R. A. *J. Phys. Chem.* **1991**, *95*, 6372−6379.

(41) Weidlich, O.; Siebert, F. *Appl. Spectrosc.* **1993**, *47*, 1394−1400.

(42) Lohrmann, R.; Grieger, I.; Stockburger, M. *J. Phys. Chem.* **1991**, *95*, 1993−2001.

(43) Hage, W.; Kim, M.; Frei, H.; Mathies, R. A. *J. Phys. Chem.* **1996**, *100*, 16026−16033.

(44) Weidlich, O.; Schalt, B.; Friedman, N.; Sheves, M.; Lanyi, J. K.; Brown, L. S.; Siebert, F. *Biochem.* **1996**, *35*, 10807−10814.

(45) Ujj, L.; Zhou, Y.; Sheves, M.; Ottolenghi, M.; Atkinson, G. H., submitted to *J. Am. Chem. Soc.*, in press.

(46) Ye, T.; Friedman, N.; Gat, Y.; Atkinson, G. H.; Sheves, M.; Ottolenghi, M.; Ruhman, S. *J. Phys. Chem.* **1999**, *103*, 5122−5130.

(47) Ben-Nun, M.; Molnar, F.; Lu, H.; Phillips, J. C.; Martinez, T. J.; Schulten, K. *Faraday Discuss.* **1998**, *110*, 447−462.

(48) Ben-Nun, M.; Martinez, T. J. *J. Phys. Chem.* **1998**, *103*, 9607−9617.